UNIVERSITY OF ZIELONA GÓRA

CIVIL AND ENVIRONMENTAL ENGINEERING REPORTS

E-ISSN 2450-8594

CEER 2024; 34 (3): 0120-0135
DOI: 10.59440/ceer/190839

Original Research Article

ARTIFICIAL NEURAL NETWORK-AIDED MATHEMATICAL MODEL FOR PREDICTING SOIL STRESS-STRAIN HYSTERESIS LOOP EVOLUTION

Marta BOCHEŃSKA[1], Piotr SROKOSZ
Faculty of Geoengineeing, Institute of Geodesy and Civil Engineering, University of Warmia and Mazury in Olsztyn, Olsztyn, Poland

A b s t r a c t

This study presents a novel approach to forecasting the evolution of hysteresis stress-strain response of different types of soils under repeated loading-unloading cycles. The forecasting is made solely from the knowledge of soil properties and loading parameters. Our approach combines mathematical modeling, regression analysis, and Deep Neural Networks (DNNs) to overcome the limitations of traditional DNN training. As a novelty, we propose a hysteresis loop evolution equation and design a family of DNNs to determine the parameters of this equation. Knowing the nature of the phenomenon, we can impose certain solution types and narrow the range of values, enabling the use of a very simple and efficient DNN model. The experimental data used to develop and test the model was obtained through Torsional Shear (TS) tests on soil samples. The model demonstrated high accuracy, with an average R^2 value of 0.9788 for testing and 0.9944 for training.

Keywords: deep neural networks, hysteresis loops, mathematical modeling, soil stress-strain curves, cyclic loading

1. INTRODUCTION

Modeling of soil mechanical response is a fundamental challenge in geotechnical engineering. Advanced constitutive models can capture the intricate behavior of soils, but their complexity often limits practical applications. For design applications the models usually need to be radically simplified and the material properties and loading models are idealized. Although the simplified versions of constitutive laws are easier to use in practice, they do not capture the nature of modeled phenomenon and might produce results affected by major errors when used for modeling complex soil-structure interactions.

What is more, the decision on which constitutive model to use for a specific practical case is not straightforward. In (Lade 2005) over 30 widely available models were presented and compared, and

[1] Corresponding author: Faculty of Geoengineeing, Institute of Geodesy and Civil Engineering, University of Warmia and Mazury in Olsztyn, e-mail: marta.bochenska@uwm.edu.pl

practical aspects of their evaluation were also taken into account. The models were divided into several different groups according to the frameworks and the key attributes, such as the shapes of the failure, yield, and plastic potential surfaces as well as the hardening parameters. Along with the capabilities of each model, the experiments required to calibrate their parameters are given. The study showed that the possibilities and disadvantages of constitutive models are not always easy to ascertain, and the models differ in the required parameters determining. This complexity has led researchers to explore artificial intelligence (AI) techniques as an alternative.

Artificial neural networks (ANN), offer a way to develop material behavior models directly from laboratory test results without explicitly formulating constitutive relations. The use of ANNs in constitutive modeling began in the 1990s, focusing on pattern recognition in experimental data. Early applications included modeling the behavior of various geomaterials such as soil (Ellis et al. 1995; Wu 1997), rock (Millar and Clarici 1994; Zhang et al. 1991), and concrete (Sankarasubramanian and Rajasekaran 1996).

By the late 1990s, practical applications emerged, integrating ANN-based models into Finite Element (FE) methods for practical applications. Pande and Shin (2002) developed FE codes with ANN-based constitutive models for risk assessment and long-term structural performance monitoring, including critical structures like dams and nuclear facilities. Javadi and colleagues (Javadi 2003; Javadi et al. 2009) confirmed the usefulness of ANNs for simple tasks with linear-elastic, non-linear-elastic, and elastic-plastic stress-strain relations. It is important to note that the prediction accuracy depends not only on the quantity and the quality of training data but also on the network architecture (Bagińska and Srokosz 2019).

Recent studies concerning ANNs techniques in geotechnical engineering include cohesion of sandy soils reinforced with fibers (175), identifying the dispersibility of soils (182), hydraulic conductivity in soils (183), forecast the bearing capacity of driven piles in cohesionless soil (185) or predicting the shear strength of soil reinforced with fibers (191).

Also, in recent years AI techniques have expanded beyond ANNs to include Machine Learning (ML), Deep Learning (DL), and Ensemble Learning (EL). These techniques have shown significant promise in geotechnical engineering due to their ability to model intricate and nonlinear processes without presuming initial input-output relationships (Baghbani et al., 2022; Beiranvand and Rajaee, 2022). ML techniques are particularly valued for their high interpretability and optimal performance with small data sets, making them suitable for tasks such as soil classification, spatial property variability prediction, and slope stability assessment (Assadi-Langroudi et al., 2022).

Deep Learning (DL), a subset of ML, enhances learning algorithms' capability to comprehend complex data using neural networks with multiple layers of interconnected nodes. DL techniques are effective in handling large volumes of data and identifying complex patterns, making them suitable for geological feature detection, landslide prediction, seismic data analysis, and infrastructure monitoring (Lee et al., 2003).

Ensemble Learning (EL) techniques, which combine multiple ML models to improve predictive accuracy, have been shown to outperform individual models in many geotechnical applications. EL methods are used for forecasting soil liquefaction susceptibility, categorizing rock mass quality, estimating lateral wall deflection in braced excavations, and predicting soil properties from raw soil spectra data (Samui, 2020).

Modeling soil behavior under cyclic loading, characterized by stress-strain hysteresis and changing soil parameters, is a challenging task, even when using AI methods. Thus in this study we propose a novel approach to predict soil stress-strain curves resulting from multiple loading cycles based solely on soil properties and loading parameters.

It is important to emphasize that traditional methods for approximating soil behavior, such as the generalized hyperbolic equation (Kondner 1963; Kondner and Zelasko 1963) and its modifications (Duncan and Chang 1970; Hardin and Drnevich 1972; Nogami et al. 2012; Puzrin 2012), and the logarithmic function (Puzrin and Burland 1996), do not account for the evolution of hysteresis loops with subsequent loading cycles.

Therefore we combine mathematical modeling, regression analysis, and Deep Neural Networks (DNNs) to forecast the evolution of hysteresis stress-strain response of different soil types under repeated loading-unloading cycles, offering a tool for geotechnical engineering applications. In more detail, we propose a hysteresis loop evolution equation and design a family of DNNs to obtain parameters of the equation. Our assumption was that this model would be able to effectively predict soil mechanical response with minimal data and simulate the phenomenon accurately. The results confirmed our assumptions, demonstrating the model's capability to describe effectively the evolution of the hysteresis loop given only soil and loading parameters.

To develop and validate the model, a series of laboratory experiments using Torsional Shear (TS) tests were conducted. Fifteen series were used for model development and four for testing. The choice of the equation's complexity was crucial; an overly complex equation could hinder regression and training algorithms, while an overly simple equation could result in significant errors.

2. TORSIONAL SHEAR (TS) DEVICE

The TS apparatus is a precision measuring device designed to perform both resonant column and torsional shear tests. It has been applied in geotechnical engineering across the world since the 1960s. The TS device used in this study is the WF8500 model manufactured by Wykeham Farrance. The WF8500 is a dual function device. It enables soil sample testing with low frequency torsion oscillation (the TS mode) and resonant frequency detection (the resonant column mode, RC mode). In most cases, the device is used to determine the elasticity parameters related to soil stiffness (such as the deformation modulus G and damping ratio D). The device operates in the frequency range of 0.01-300 Hz and in the range of angular amplitudes from 0.01-30 mRad. This allows for the generation of small and very small shear deformations. The main control parameters of the TS test are frequency, amplitude and number of load cycles. The initial stress state, saturation and isotropic consolidation processes are controlled by the confining pressure, which is applied by means of compressed air, through the water jacket (Fig. 1). The device is powered and controlled by an external driver connected to the computer. The driver is operated using specialized DYNATOR software. The software enables:

- performing multiple TS tests on the same soil sample,
- fully automated results processing,
- smooth adjustment of the deformation level and the confining pressure adjustments.

In the TS mode, the device cyclically loads the sample with a harmonically changing torque T and measures the shear angle Θ. The torque is generated by an electromagnetic actuator, and the angle is measured by a pair of inductive proximity sensors (Fig. 1). The load is applied to the free upper end of the sample, the lower end is fixed (attached to the base of the chamber of the device, Fig. 2). The boundary conditions reflect the Kelvin-Voigt SDOF model.

The shear stress τ is given by the formula

$$\tau = \kappa \frac{TR}{J} \tag{2.1}$$

where R - sample radius, J - geometrical moment of inertia, κ - averaging factor (0.6-0.8).

Shear strain is calculated using the following formula

$$\gamma = \frac{\Theta r}{H} \tag{2.2}$$

where H is the sample height and $r=\kappa R$. The hysteresis loop $\tau(\gamma)$ is a typical TS test result.

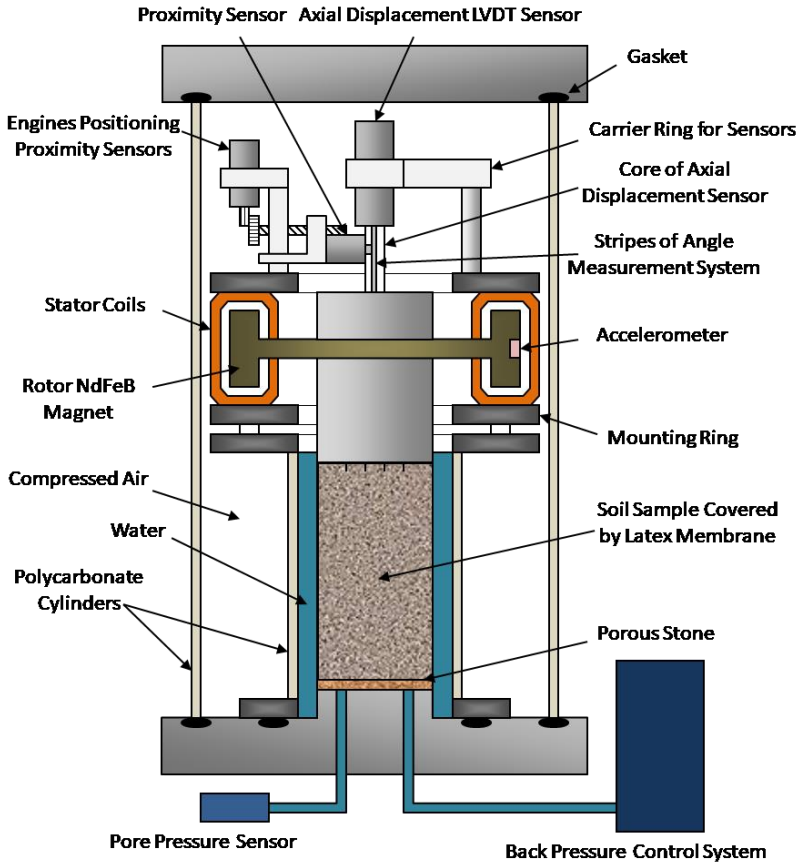

Fig. 1. Schematic drawing of the Torsional Shear device

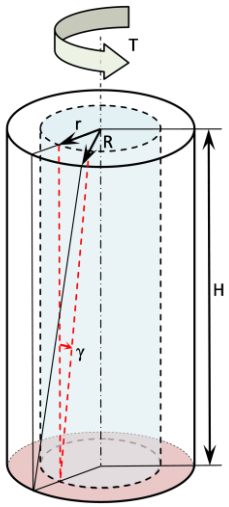

Fig. 2. Idealized model of a soil specimen under Torsional Shear test

3. DESCRIPTION OF THE MODEL

The main objective of this study was to propose and evaluate an effective way to model stress-strain (τ-γ) response of soil due to repeated loading-unloading cycles. Therefore the model should transform discrete set of data (soil parameters; pore and cell pressure; amplitude and frequency of applied cyclic loading, see Tab. 2 for complete set of parameters) into continuous subset of $\mathbb{R}^2$(hysteresis loops).

$$\left\{\begin{matrix} diameter, & height, \\ weight, & frequency, \\ amplitude, & cell\ pressure, \\ pore\ pressure, & axial\ deformation \end{matrix}\right\} \mapsto \left\{\begin{matrix} evolution\ of \\ hysteresis \subset \mathbb{R}^2 \end{matrix}\right\} \tag{3.1}$$

This is done in the following steps

- Develop a hysteresis loop evolution model.
- Transform experimental data into model parameters.
- Use neural networks to predict model parameters.
- Compare results obtained in the two previous steps (test the accuracy of the prediction).

3.1. Model of a hysteresis loop evolution

One of the simplest hysteresis loop models is given by the following set of equations (see for example Lapshin 1995)

$$\gamma_1(t) = 4Pcos^m(t) + Qsin^n(t), \tag{3.2}$$

$$\tau(t) = Rsin(t) \tag{3.3}$$

where P, Q, $R \in \mathbb{R}$ are constants. Note that to obtain the "classical" hysteresis loop one can put n=m=3 (see Fig. 3). In our case Eq. 3.2 may be written in the form

$$\gamma_1(t) = p(3\cos(at+b) + \cos(3at+3b)) + q(3\sin(at+b) - \sin(3at+3b)) \tag{3.4}$$

The above function is $\frac{2\pi}{a}$-periodic and thus cannot produce a loop with geometry changing in time. Therefore we propose the following modification

$$\gamma(t) := f(t)\gamma_2(t), \tag{3.5}$$

$$\gamma_2(t) = qcos(3at + 3b) + wcos(at + b) + psin(at + b) + ksin(3at + 3b) \tag{3.6}$$

where *f(t)* is a scaling function corresponding to evolution of the hysteresis loop. In our study we take

$$f(t) = A + \frac{B}{x + C} \tag{3.7}$$

where *A, B* are constants depending on the sample and *C* is set to be equal 500 for all samples (this value of *C* gives the best results). The parameters *a, b, p, q, k, w* are model constants. These parameters are analogous to the weights in a neural network, and their values are determined through a process similar to neural network training.
Therefore to model a stress response of a given soil sample one should find the parameters *a, b, p, q, k, w, A, B* $\in \mathbb{R}$. This can be done using regression analysis.

In our study we use Levenberg-Marquardt algorithm to find the required set of parameters $\hat{\beta}$: {a, b, p, q, k, w, A, B} (see for example Pujol 2007) describing experimental data. That is, $\hat{\beta}$ is such set of parameters of γ so that γ optimally describes the experimental data. Therefore the set $\hat{\beta}$ should minimize the following function

$$S: \mathbb{R}^8 \to \mathbb{R}, S(\beta) := \sum_{i=1}^{m} (y_i(t_i) - \gamma(t_i, \beta))^2 \tag{3.8}$$

where $y_i(t_i)$ is the set of experimental points (obtained using TS device).
The Levenberg-Marquardt algorithm is an iterative procedure. In each step β is replaced by a vector $\beta + \delta$. As δ is small (in a small neighbourhood of $0 \in \mathbb{R}^8$ thus

$$\gamma(t_i, \beta + \delta) \approx \gamma(t_i, \beta) + J_i\delta \tag{3.9}$$

where $J_i = \nabla f(\beta)$ is the gradient. Thus in the matrix notation we have

$$S(\beta + \delta) \approx \|\mathbf{y} - \Gamma(\beta) - \mathbf{J}\delta\|^2 \tag{3.10}$$

where ||.|| denotes the standard Euclidean norm. Also **y**, Γ (β) and **J** are $m \times 8$ matrices with *i*-th row equal to y_i, $\gamma(x_i, \beta)$ and J_i, respectively. To find a local minimum we can differentiate *S* w.r.t. δ and set the result to zero. This yields the following condition

$$(\mathbf{J}^T\mathbf{J})\delta = \mathbf{J}^T(\mathbf{y} - \mathbf{f}(\beta)) \tag{3.11}$$

In the Levenberg-Marquardt algorithm one modifies the above equation by adding the so-called *damping factor* λ

$$(\mathbf{J}^T\mathbf{J} + \lambda\mathbb{I})\delta = \mathbf{J}^T(\mathbf{y} - \mathbf{f}(\beta)) \tag{3.12}$$

where $\mathbb{I} \in M_{8\times8}(\mathbb{R})$ is the identity matrix.

As one can see this algorithm detects local minima and thus finds only local optimums. In our study the parameters obtained by the algorithm with random β are useless (see Fig. 5 for an example). Therefore it is crucial to feed the algorithm with adequate starting set of parameters β. Therefore we use the following procedure

1. Find parameters A', B' of $f(t)$. Take the experimental data ($\gamma_e(t_i)$) and find points (t_k, $\gamma_e(t_k)$), $1 \le k \le n$ which

correspond to the extremes. Use Levenberg-Marquardt algorithm to find A', B' corresponding to points $\{(t_{ik}, |\gamma_e(t_k)|)\}$ (see Fig. 4).

2. Find parameters a', b' by fitting a curve $\frac{1}{f(t)}\sin(a't + b')$ $ to the experimental data.
3. Put obtained parameters A', B', a', b' into $\gamma(t)$ and find p', q', k', w' again, using Levenberg-Marquardt algorithm.
4. Use Levenberg-Marquardt algorithm with starting set $\beta=\{a', b', p', q', k', w', A', B'\}$.

An example obtained using our procedure is given in Fig. 6. The algorithm was implemented in MATLAB.

Thus the modelling process can be reduced to predicting the parameters of γ

$$\left\{\begin{matrix} diameter, & height, \\ weight, & frequency, \\ amplitude, & cell\ pressure, \\ pore\ pressure, & axial\ deformation \end{matrix}\right\} \mapsto \left\{\begin{matrix} a, b, p, q, k, w, \\ A, B \end{matrix}\right\} \tag{3.13}$$

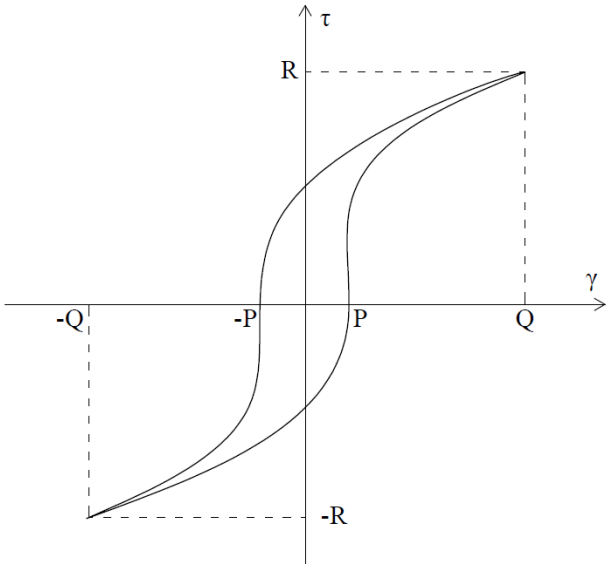

Fig. 3. Classical hysteresis loop

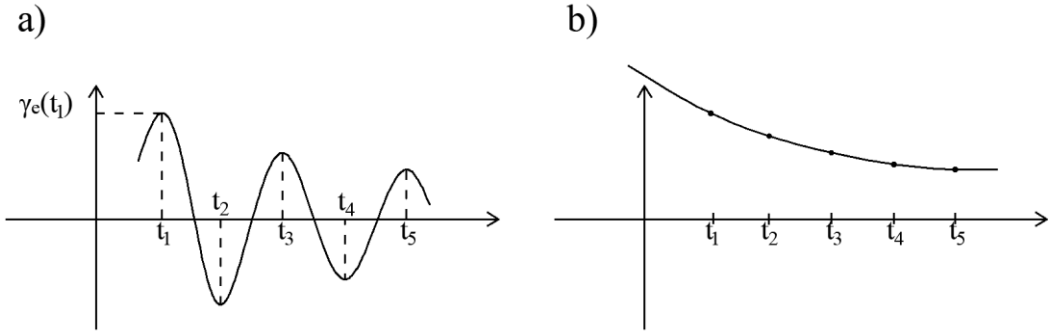

Fig. 4. A schematic graphs: a) experimental data $\boldsymbol{\gamma_e(t)}$, b) points $\boldsymbol{t_k}$,$\boldsymbol{\gamma_e(t_k)}$ corresponding to the extremes of the experimental data

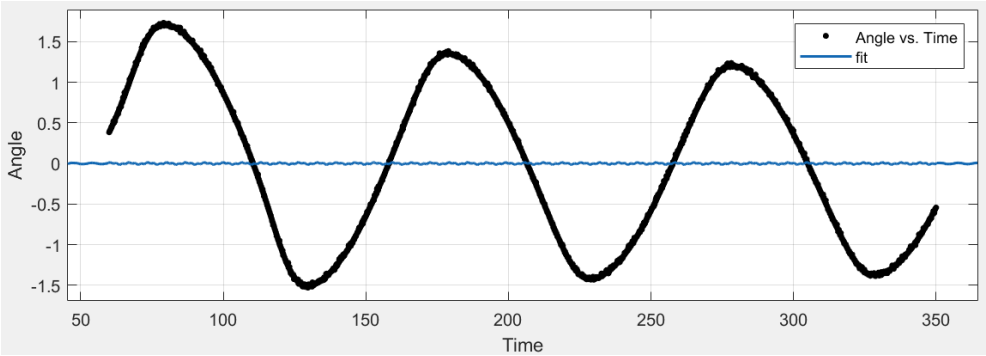

Fig. 5. A fitted curve with the curve parameters obtained by the algorithm with random $\boldsymbol{\beta}$

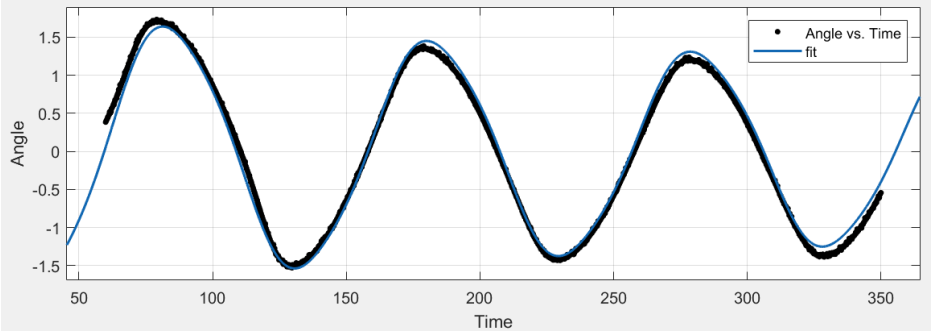

Fig. 6. An example of fit obtained using the procedure proposed in this study

3.2. Deep neural networks

To predict the parameters of γ based on soil parameters, pore and cell pressure, amplitude and frequency of applied cyclic loading we use Deep Neural Networks (DNNs).

A *DNN* is an artificial neural network (ANN), that is a computing system consisting of interconnected processing units (neurons) arranged into specialized layers (input layer, hidden layers, output layer). It can be trained to approximate multivariable functions. In the training process an ANN generates a model for input-output relations by analysing training data samples and adjusting connection weights according to a gradient of an error function. Properly trained ANN can make accurate output predictions for non-training input data. The training effectiveness is highly correlated with the quantity and quality of training data, the network architecture and the training parameters.

To obtain the output vector each coordinate of the input vector is multiplied by a corresponding weight and added up together. The weighted sum is then used to calculate the value of an activation function. The activation function is a real function that determine the value returned by neurons in the output layer (e.g. logistic function, hyperbolic functions (tanh), inverse trigonometric functions (arctan), softsign).

The ANN architecture can be one of two general types, feedforward (the data is processed one time by the same neuron) or recurrent (connection loops can be formed).

The most common feedforward type of network is a multilayer perceptron (MLP). An MLP has three layers at least (1 input, 1 hidden, 1 output). An MLP network with more than two hidden layers is called the *deep* neural network.

Due to additional connections complex relations can be modelled more precisely using fewer neurons (Baral et al., 2018). Therefore in this study the model was developed using deep learning.

The DNNs used in this study are prepared using MATLAB environment. The architecture of the networks is given in Fig. 7. As the training set is relatively small (15 samples) the architecture and parameters of the DNNs were chosen based on the research conducted by the authors of this paper (Bagińska and Srokosz 2019). In more detail we use

- Bayesian regularization as a training algorithm,
- log-sigmoid activation function

$$\text{logsig}(n) = \frac{1}{(1+\exp(-n))}, \tag{3.14}$$

- maximum number of training epochs 200,
- maximum number of consecutive fails (increases in error) during the training process 5.

For the prediction of each parameter *a*, *b*, *p*, *q*, *k*, *w*, *A*, *B* 200 DNNs were trained and the one with best training performance was used in the experiment.

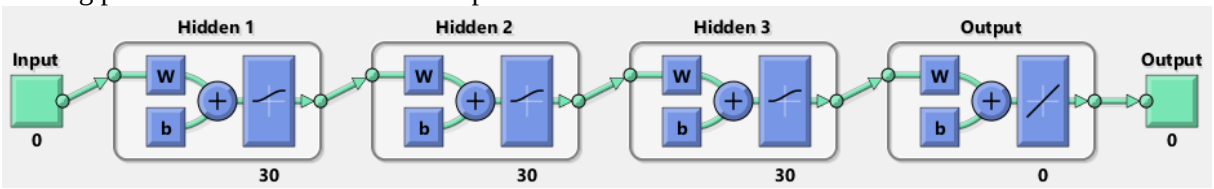

Fig. 7. A single DNN architecture

4. RESULTS

The experimental data used for the model development and evaluation were obtained with torsional shearing tests of different soils. The parameters of the soils tested in the TS device are given in Tab. 1.

Table 1. Parameters of tested soils

Soil	Specific gravity	Nominal particle size d_{50} [mm]	Uniformity coefficient C_U [-]	Void ratio *e* [-]	Volumetric density ρ [kg/m3]	Compaction/consistency index *Cc/CI* [-]
Sandy silt (saSi)	2.66	0.047	17.1	0.67	1870	0.11
Medium sand (MSa) 1	2.65	0.33	2.6	0.42	1860	0.97
Medium sand 2	2.65	0.33	4.0	0.37	1930	0.94

Table 2. Specimen and TS test parameters

Specimen label	Soil	Diameter [mm]	Height [mm]	Weight [mm]	Frequency [Hz]	Amplitude [V]	Cell pressure [kPa]	Pore pressure (avg.) [kPa]	Axial [mm]
R19	saSi	68.9	144.3	1212.68	0.05	9	50	-3.33	8.7
R16	saSi	68.9	144.8	1213.14	0.05	2	50	-4.34	8.7
R18	saSi	69.0	144.2	1213.03	0.05	7	50	-3.93	8.7
R24	saSi	68.9	144.8	1213.42	0.05	8	50	-3.84	8.7
R27	saSi	69.0	144.4	1213.17	0.05	1	50	-4.38	8.7
R29	saSi	69.0	144.3	1212.97	0.05	10	50	-3.22	8.7
R36	saSi	68.9	144.5	1212.88	0.05	3	50	-4.24	8.7
R37	saSi	69.0	144.2	1213.24	0.05	0.5	50	-5.03	8.7

R40	saSi	68.9	144.6	1213.47	0.05	4	50	-4.19	8.7
R43	saSi	68.9	144.6	1213.45	0.05	6	50	-3.99	8.7
R50	saSi	68.9	144.7	1213.29	0.05	5	50	-4.16	8.7
G35	MSa 2	72.8	143.1	1093.00	0.01	5	49.7	1.29	5.53
G13	MSa 2	72.8	143.0	1093.10	0.01	7	49.7	1.33	5.53
G10	MSa 2	72.7	143.1	1092.77	0.01	10	49.9	1.34	5.53
G33	MSa 2	72.7	143.0	1092.80	0.01	10	103.5	1.31	5.53
B19	MSa 1	70.0	143.1	1029.00	0.01	9	27.9	0.60	5.86
B16	MSa 1	70.0	143.2	1029.00	0.01	9.7	27.7	-0.64	5.78
B26	MSa 1	70.0	143.3	1029.60	0.01	9.5	351.8	-0.52	5.72
B57	MSa 1	70.0	143.3	1029.30	0.01	9.2	400.0	-0.60	5.77

The parameters of each soil specimen and the test parameters are presented in Tab. 2. The TS tests were carried out with low frequency of changing torque (0.01-0.05 Hz).

4.1. Training samples

For the DNNs' training 15 out of 19 samples were used (9 samples of saSi, 3 of MSa 1 and 3 of MSa 2).

The parameters of the function fitted to the raw experimental results ($\gamma(t)$) are given in Tab. 3. Tab.

$$R^2 = 1 - \frac{\sum_{i=1}^{n}(\widehat{y_i} - y_i)^2}{\sum_{i=1}^{n}(y_i - \bar{y})^2}, \tag{4.1}$$

4 presents goodness of that fit measured by R^2.
where y_i are the experimental dataset values, $\widehat{y_i}$ are the fitted values and

$$\bar{y} = \frac{1}{n}\sum_{i=1}^{n} y_i \tag{4.2}$$

Table 3. Model parameters obtained with regression

Specimen label	A	B	b_1	c_1	k	p	q	w
R16	0.471	-29.29	0.314	3.032	0.000	1.000	-0.003	0.002
R24	3.525	-327.4	0.314	2.962	0.023	1.023	-0.009	0.001
R36	0.957	-135.2	0.314	3.010	0.003	1.002	-0.004	-0.001
R43	2.689	-418.7	0.314	2.966	0.015	1.014	-0.008	0.002
R37	0.090	0	0.314	3.067	-0.003	1.005	0.001	-0.002
R50	2.043	-309.1	0.314	2.979	0.012	1.008	-0.007	0.002
R27	0.205	-9.049	0.314	3.059	-0.002	0.984	-0.002	-0.001
R29	3.930	-148.7	0.314	2.968	0.043	1.054	-0.009	0.000
R40	1.464	-218.3	0.314	2.993	0.007	1.007	-0.006	-0.001
G10	-0.304	1928.0	0.064	2.520	0.034	1.022	-0.051	-0.015
G35	-0.026	648.2	0.064	2.575	0.004	0.996	-0.037	-0.013
G33	-0.489	1217.0	0.064	2.576	0.033	1.016	-0.029	-0.018
B19	1.061	542.7	0.314	2.812	0.006	1.003	-0.025	-0.005
B16	1.537	167.5	0.314	2.911	0.023	1.034	-0.023	-0.002
B57	0.366	-9.824	0.314	3.063	0.002	1.007	-0.003	0.001

Table 4. Model parameters predicted by the DNNs

Specimen label	A	B	b_1	c_1	k	p	q	w
R19	3.823	-308.8	0.314	2.955	0.035	1.043	-0.009	0.0002
R18	2.395	-29.53	0.315	2.962	0.024	1.033	-0.008	-0.0004
G13	-0.154	1110.0	0.064	2.938	0.013	1.001	-0.043	-0.015
B26	0.578	-92.23	0.062	3.066	0.009	1.015	-0.004	0.002

Table 5. Goodness of fit

Specimen label	R^2
R16	0.9997
R24	0.9995
R27	0.9989
R29	0.9995
R36	0.9998
R37	0.9941
R40	0.9998
R43	0.9998
R50	0.9999
G10	0.9928
G33	0.9748
G35	0.9781
B16	0.9995
B19	0.9974
B57	0.9997

Table 6. Goodness of fit of the DNN model

Specimen label	R^2
R16	0.9992
R18	0.9988
G13	0.9885
B26	0.9286

4.2.Test samples

For the DNNs' testing 4 of 19 data samples were used (2 of saSi, 1 of MSa 1 and 1 of MSa 2). Model parameters predicted by the DNN unit are given in Tab. 5 and the goodness of fit of the obtained function to the experimental data is presented in Tab. 6. Figures 8-11 present the results obtained with the proposed model, i.e. the stress-strain curves and the evolution of the hysteresis loops through three loading-unloading cycles.

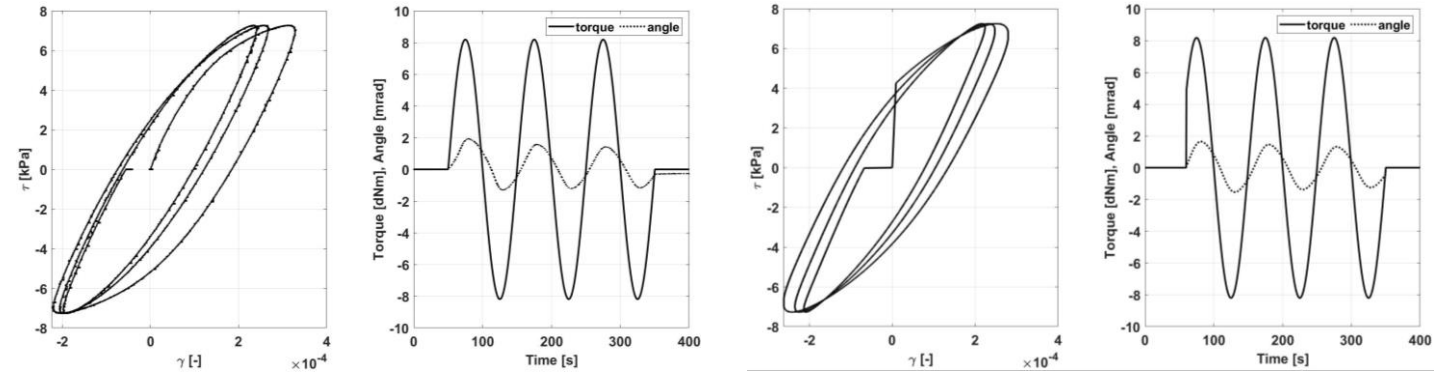

Fig. 8. Results for specimen G13 (MSa 2). Experiment (on the right) vs. model (left)

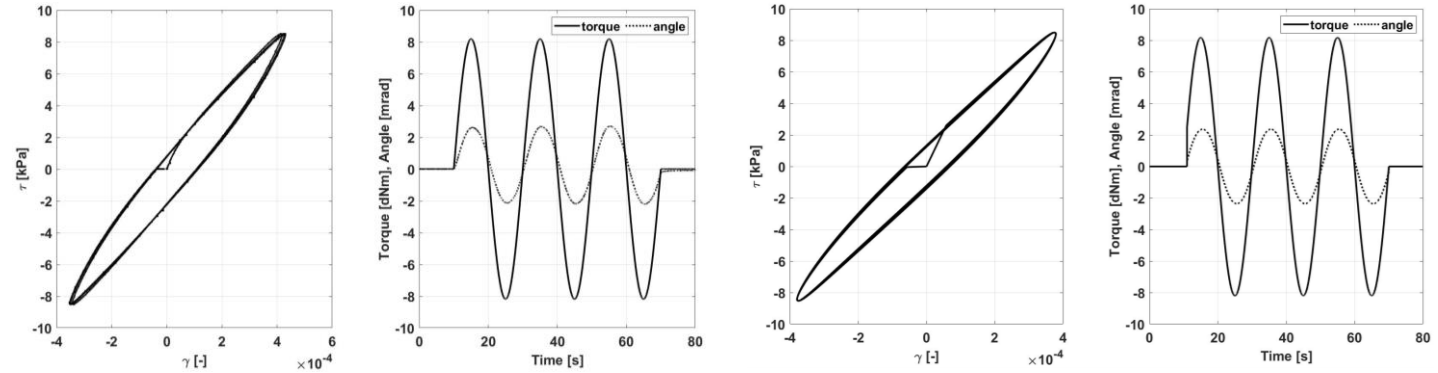

Fig. 9. Results for specimen R18 (saSi). Experiment (on the right) vs. model (left)

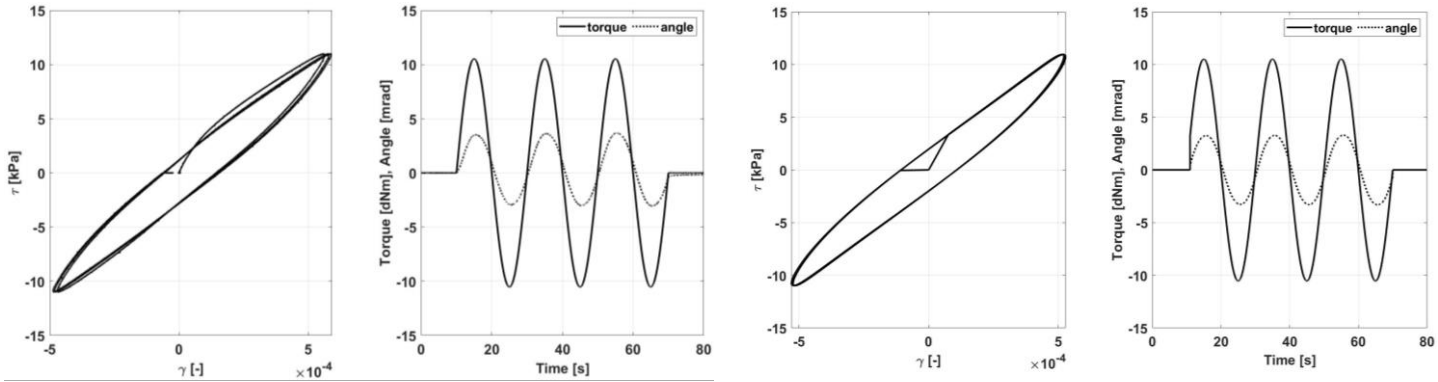

Fig. 10. Results for specimen R19 (saSi). Experiment (on the right) vs. model (left)

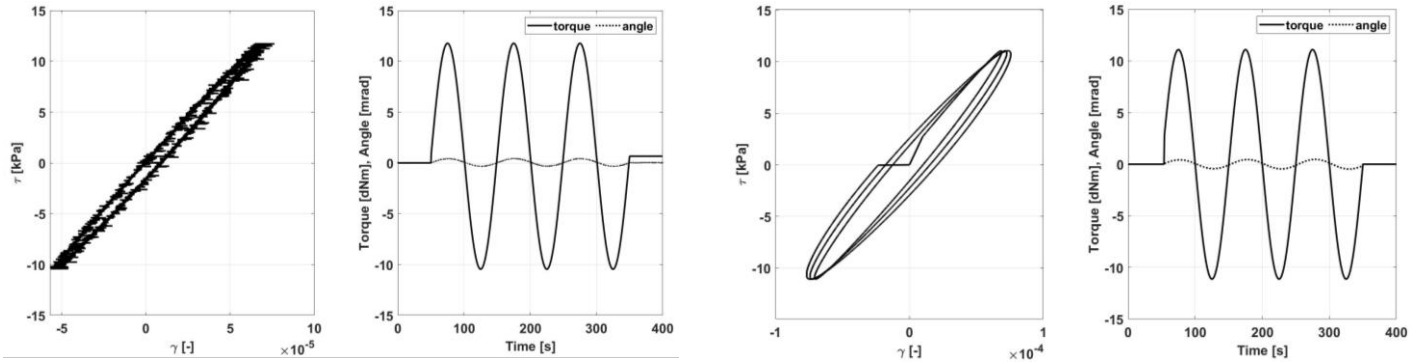

Fig. 11. Results for specimen B26 (MSa 1). Experiment (on the right) vs. model (left)

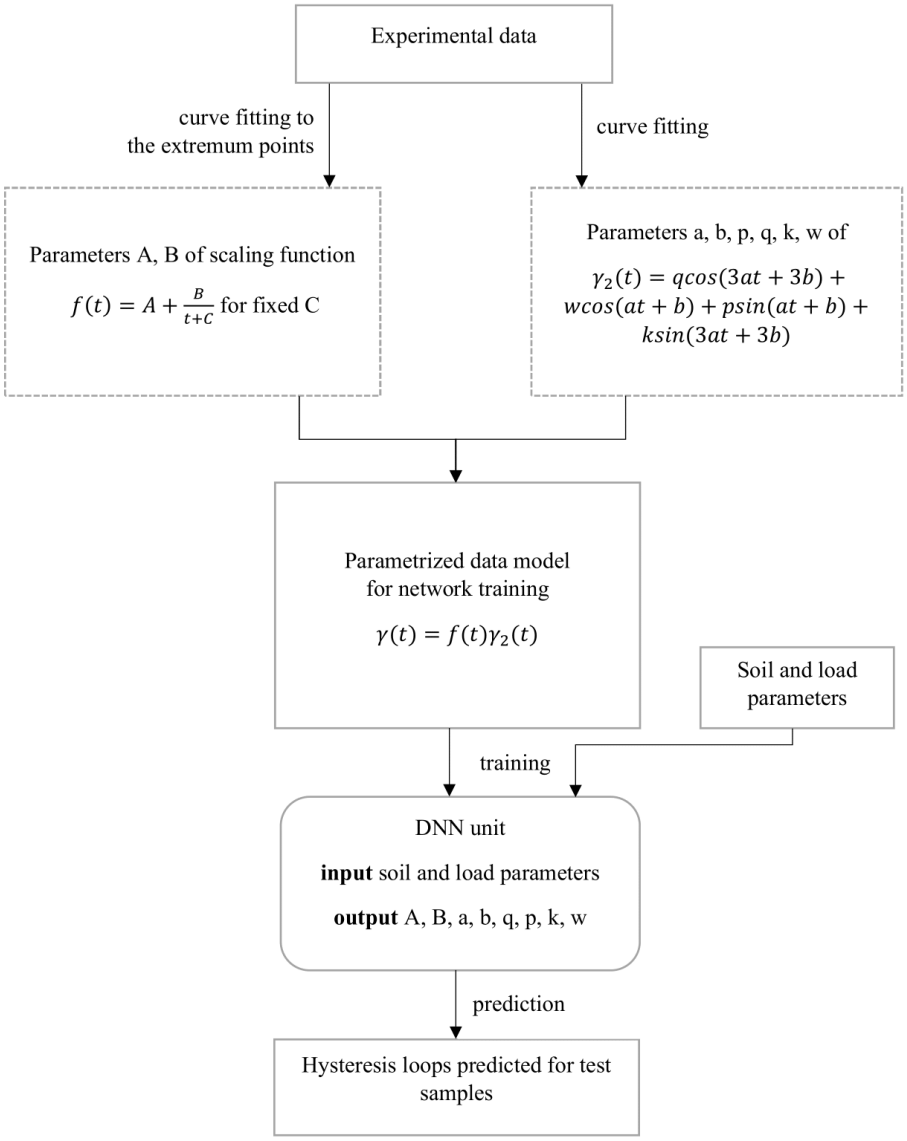

Fig. 12. Proposed procedure flowchart

5. CONCLUSIONS AND RECOMMENDATIONS

The following main conclusions can be drawn from this study:

1. **Model accuracy:** The results obtained with the proposed model show good compliance with the experimental data with R2 values ranging from 0.9286 to 0.9992. This high level of accuracy is noteworthy, especially considering that:
    - the prediction was made solely from the knowledge of the soil properties and the loading parameters,
    - the training dataset was relatively small.
2. **Support for modeling methods:** While ANN models may not always be used as independent tools for modeling and predicting complex material behavior, they can effectively support other modeling methods. Neural network-based approaches can be integrated into analytical models, aiding their development and potentially simplifying their application in engineering practice.
3. **Efficiency and practicality:** By combining DNNs with mathematical modeling, the study demonstrates that an efficient model can be created, capable of accurately modeling the phenomenon and predicting results with minimal data. This hybrid approach is particularly useful in practical applications where experimental data may be limited.
4. **Experimental validation:** The validation through laboratory experiments using Torsional Shear (TS) tests confirmed the model's reliability in simulating the mechanical response of various soil types under repeated loading-unloading cycles.

Recommendations

1. **Implementation in engineering practice:** The developed hybrid model might be considered for implementation in geotechnical engineering projects where accurate soil behavior predictions are critical. This includes applications such as foundation design, slope stability analysis, and risk assessment of critical structures.
2. **Further research:** Future studies could explore the application of this hybrid modeling approach to a broader range of soil types and loading conditions to validate and refine the model further. Additionally, investigating the integration of other AI techniques such as Ensemble Learning could enhance the model's predictive capabilities.

REFERENCES

1. Arabet L, Hidjeb M, Belaabed F, 2022. A comparative study of reinforced soil shear strength prediction by the analytical approach and artificial neural networks. *Engineering, Technology and Applied Science Research* **12(6)**, 9795–9801.
2. Armaghani DJ, Mirzaei F, Shariati M, Trung NT, Shariati M and Trnavac D, 2020. Hybrid ANN-based techniques in predicting cohesion of sandy-soil combined with fiber. *Geomechanics and Engineering* **20(3)**, 191–205.
3. Assadi-Langroudi A et al., 2022. Recent advances in nature-inspired solutions for ground engineering (NiSE). *International Journal of Geosynthetics Ground Engineering* **8(1)**, 3.
4. Baghbani A, Choudhury T, Costa S and Reiner J, 2022. Application of artificial intelligence in geotechnical engineering: a state-of-the-art review. *Earth-Science Reviews* **228**, 103991.
5. Bagińska, M and Srokosz, PE, 2019. The optimal ANN model for predicting bearing capacity of shallow foundations trained on scarce data. *KSCE Journal of Civil Engineering*, **23(1)**, 130-137. https://doi.org/10.1007/s12205-018-2636-4
6. Baral, C, Fuentes, O and Kreinovich V, 2018. Why deep neural networks: a possible theoretical explanation. In: Ceberio M, Kreinovich V (eds) Constraint Programming and Decision Making: Theory and Applications. Studies in Systems, *Decision and Control*, vol 100. Springer, Cham. https://doi.org/10.1007/978-3-319-61753-4_1
7. Beiranvand B, Rajaee T, 2022. Application of artificial intelligence-based single and hybrid models in predicting seepage and pore water pressure of dams: a state-of-the-art review. *Advances in Engineering Software* **173**, 103268.
8. Duncan, JM and Chang CY, 1970. Non-linear analysis of stress and strain in soils. *Journal of Geotechnical Engineering (ASCE)*, **96(5)**, 1629-1653.
9. Ellis, GW, Yao, C, Zhao, R and Penumadu, D, 1995. Stress-strain modeling of sands using artificial neural networks. *Journal of Geotechnical Engineering, ASCE* **121(5)**, 429-35.
10. Hardin, BO and Drnevich, VP, 1972. Shear modulus and damping in soils: design equations and curves. *Journal of the Soil Mechanics and Foundations Division (ASCE)*, **98(SM7)**, 667-691.
11. Javadi, AA, Mehravar, M, Faramarzi, A and Ahangar-Asr, A, 2009. An artificial intelligence based finite element method. *ISAST Transactions on Computers and Intelligent Systems*, **1(2)**, 1-7.
12. Javadi, AA, Tan, TP and Zhang, M, 2003. Neural network for constitutive modelling in finite element analysis. *Computer Assisted Mechanics and Engineering Sciences*, **10(4)**, 523-529.
13. Kondner, RL, 1963. Hyperbolic stress-strain response: cohesive soils. *Journal of the Soil Mechanics and Foundations Division (ASCE)*, **89(SM1)**, 115-143.
14. Kondner, RL and Zelasko, JS, 1963. *A hyperbolic stress-strain formulation of sands*. Proceedings of 2nd Pan American Conference on Soil Mechanics and Foundation Engineering, Brazilian Association of Soil Mechanics, São Paulo, 289-324.
15. Lade, PV, 2005. Overview of constitutive models for soils. ASCE Geotechnical Special Publication No. 128, Soil Constitutive Models: Evaluation, Selection, and Calibration, Edited by JA Yamamuro and VN Kaliakin, January, 1-34.
16. Lapshin, RV, 1995. Analytical model for the approximation of hysteresis loop and its application to the scanning tunneling microscope. *Review of Scientific Instruments*, **66**, 4718-4730.
17. Lee S, Lee SR and Kim Y, 2003. An approach to estimate unsaturated shear strength using artificial neural network and hyperbolic formulation. *Compututers and Geotechnics* **30(6)**, 489–503.
18. Millar, D and Clarici, E, 1994. *Investigation of backpropagation artificial neural networks in modeling the stress-strain behavior of sandstone rock.* Proceedings of 1994 IEEE International Conference on Neural Networks, IEEE Service Center, 3326-3331.

19. Nogami, Y, Murono, Y and Morikawa, H, 2012. *Nonlinear hysteresis model taking into account S-shaped hysteresis loop and its standard parameters.* Proceedings of the 15th World Conference of Earthquake Engineering, Lisboa.
20. Pande, GN and Shin, HS, 2002. Finite elements with artificial intelligence, In: *Numerical Models in Geomechanics - NUMOG VIII*, Swets and Zeitlinger, Lisse, 241-246.
21. Pujol, J, 2007. The solution of nonlinear inverse problems and the Levenberg-Marquardt method. *Geophysics SEG*. **72(4)**, W1-W16. https://doi.org/10.1190/1.2732552
22. Puzrin, AM, 2012. *Constitutive modeling in geomechanics. Introduction*. Springer, 2012. https://doi.org/10.1007/978-3-642-27395-7
23. Puzrin, AM and Burland, JB, 1996. A logarithmic stress-strain function for rocks and soils. *Geotechnique*, **46(1)**, 157-164. https://doi.org/10.1680/geot.1996.46.1.157
24. Samui P, 2020. *Application of artificial intelligence in geo-engineering*. In: Information technology in geo-engineering: proceedings of the 3rd international conference (ICITG), Guimarães, Portugal 3. Springer, pp 30–44.
25. Sankarasubramanian, G and Rajasekaran, S, 1996. Constitutive modeling of concrete using a new failure criterion. *Computers and Structures*, **58(5)**, 1003-1014. https://doi.org/10.1016/0045-7949(95)00200-Z
26. Shaik S, Krishna KSR, Abbas M, Ahmed M and Mavaluru D, 2019. Applying several soft computing techniques for prediction of bearing capacity of driven piles. *Engineering with Computers* **35**, 1463–1474.
27. Williams CG and Ojuri OO, 2021. Predictive modelling of soils' hydraulic conductivity using artificial neural network and multiple linear regression. *SN Applied Sciences* **3**, 1–13.
28. Wu, HC, 1997. Constitutive relation modeling for soil using finite element-neural network hybrid algorithms. In: *Computer Methods and Advances in Geomechanics*, Rotterdam: Balkema, 613-617.
29. Zhang L, Du YH, Yang XJ, Fan HH, 2022. Application of artificial neural network in predicting the dispersibility of soil. *Iranian Journal of Science and Technology – Transactions of Civil Engineering* **46(3)**, 2315–2324.
30. Zhang, Q, Song, JR and Nie, XY, 1991. Application of neural network models to rock mechanics and rock engineering. *International Journal of Rock Mechanics and Mining Sciences and Geomechanics Abstracts*, **28(6)**, 535-540.